The solvent spectral density and vibrational multimode approach to optical dephasing: Two-pulse photon echo response

Tzyy-Schiuan Yang, Peter Vöhringer,[a] David C. Arnett,[b] and Norbert F. Scherer[c]
Department of Chemistry, University of Pennsylvania, Philadelphia, Pennsylvania 19104-6323

(Received 3 May 1995; accepted 2 August 1995)

A rigorous theoretical connection between the polarizability spectral density obtained from optical Kerr effect (OKE) measurement with the correlation function describing solvent-induced optical dephasing detected in photon echo measurements is given. The experimentally obtained spectral density has a more reasonable physical basis than model correlation function descriptions of solvent fluctuations. The experimental OKE spectrum is demonstrated to provide a natural description of solvent motions that modulate the chromophore electronic states in the case of weak induced-dipolar interactions. The chromophore optically active vibrational modes are obtained from pump-probe spectra and are employed in the calculation of echo signals. It is found that the fast decays of the two-pulse echo signals result from both solvent and solute intramolecular motions while the echo peak shifts are dominated by the solvent intermolecular modes. © *1995 American Institute of Physics.*

I. INTRODUCTION

One of the interesting and fundamental challenges in understanding chemical reaction phenomena in condensed phases is obtaining the correct description of the bath and its interaction with the reactant or chromophore. The answer in solids centers around the idea of the phonon spectrum of the material.[1] The situation in liquids is significantly complicated by the lack of stable structures. The lack of a ''simply'' replicating structure makes the environment inhomogeneous from one position to another. The inherent fluctuations of the positions and orientations of the bath molecules and their interaction with the reactant or product serve as a source of excitation or dissipation. An understanding of these rapid motions and their coupling to a reaction or optical excitation coordinate is important for theoretical prediction of chemical processes in liquids.

Photon echo spectroscopy is a powerful technique to study dynamics in condensed media, where the time scales of a variety of motions occur over a very broad range (fs-ns).[2–6] The operational principle of the photon echo technique is that three sequential short laser pulses resonantly excite molecules whose absorptions lie within the laser spectral width creating a nonlinear polarization in the medium. The portion of the ensemble electronic dephasing associated with site inhomogeneity that occurs in the first period of time (i.e., between the first and second pulses) will be ''reversed'' by the polarization rephasing during the third period of time generating a coherent emission, i.e., an echo. The decay of the echo intensity with respect to the time delay between the first and second pulses reflects an irreversible dephasing process on the time scale of the measurement. The two-pulse femtosecond photon echo, where the third pulse temporally overlaps the second, can extract the fastest (system-bath and vibronic) dynamics distinguishable using finite duration laser pulses. The three-pulse photon echo is used to map out other slower motions by varying the time delay between two grating forming beams and the probe beam. Recently, two independent experiments that time-gate the photon echo signal[7–9] demonstrated that the echo shape itself is more sensitive to the solvent fluctuations than conventional time-integrated echoes. Fleming and co-workers reported fifth-order three-pulse photon echoes in contrast to time-gated echoes for elucidation of more accurate descriptions of bath correlation functions.[10,11]

In most ultrafast photon echo studies, a single or a few types of model correlation functions are used to describe the solvent fluctuations.[5,12–15] Recently, Vöhringer *et al.*[16] showed that an experimentally measured solvent vibrational spectrum provides a natural description of solvent-induced electronic fluctuations. The solute-solvent interactions in their system, the cyanine dye HITCI in polar solvents, are dominated by the ion-induced dipole and/or instantaneous dipole-induced dipole (or dispersion) forces. In the case of the chromophore studied, the solvent vibrational motions that modulate the solvent polarizability may affect the solvent-solute interactions and will, in turn, cause a modulation of the chromophore electronic energy gap. A polarizability spectrum such as is obtained from Raman scattering or the Fourier transform of optical Kerr effect (OKE) measurements provides information about these vibrational modes. The OKE measurement is especially sensitive to low frequency intermolecular collective modes and is more useful in this frequency range than a conventional Raman spectrum.[17,18]

In addition to solvent-induced dephasing, chromophore intramolecular vibrations may also play a role in shaping echo signals.[5,19–22] In femtosecond photon echo experiments, the pulse spectral width (typically several hundred cm^{-1}) is broader than low frequency molecular vibrational spacings. The optically active vibrational modes will be coherently excited upon optical excitation. The chromophore intramolecular vibrational modes are, however, usually left out in

[a]Deutsche Forschungsgemeinshaft Postdoctoral Fellow.
[b]Department of Education GAANN Predoctoral Fellow.
[c]National Science Foundation National Young Investigator.

 0021-9606/95/103(19)/8346/14/$6.00 © 1995 American Institute of Physics

Downloaded 09 Sep 2001 to 128.135.233.49. Redistribution subject to AIP license or copyright, see http://ojps.aip.org/jcpo/jcpcr.jsp

data analysis,[4,7,9,11] making interpretation of electronic dephasing somewhat ambiguous.

The purpose of this paper is two-fold. First, a detailed theoretical connection between the spectral density for optical dephasing induced by solvent fluctuations and the OKE measurement is made. The four Feynman paths contributing to the third-order polarization and finite pulse durations are included in photon echo signal calculations. Second, pump-probe transient waveforms and their Fourier spectra are used to obtain molecular vibrational information that is employed in the calculation of the photon echo signals. A pump-probe experiment directly measures the optically active vibrational modes involved in photon echo experiments. The broad spectral width of the same ultrashort pulse used in electronic dephasing measurements also generates vibrational coherences. The associated pump-probe response may show quantum beats reflecting vibrational modulation of the transition dipole moment. These oscillations provide information about vibrational frequencies in ground and/or excited electronic states, the relative potential displacements along the vibrational coordinates, and the vibrational dephasing time. Underdamped modes are used herein to model the oscillations observed in the pump-probe spectra, therefore, the chromophore's vibrational motions.

The theory and numerical calculations are applied to two-pulse time-integrated and time-gated photon echoes of HICTI and HDITC in DMSO. It is found that solvent intramolecular vibrations play an important role in the solvent-induced electronic dephasing determined in two-pulse photon echo measurements. Furthermore, by including the chromophore's vibrational contributions, the solvent-solute coupling extracted from the echo signals is about one third of that obtained by considering solvent effects only. The simulation of the spectral diffusion behavior and three-pulse photon echo dynamics of these cyanine dyes in various solvents will be reported elsewhere.[23]

II. THEORY

The idea for a two-level chromophore interacting with the set of solvent oscillators (i.e., bath) is illustrated in Fig. 1a. Here, the vertical arrows depict interactions with the applied electric fields that occur at different times (i.e., with t_1 separation). The bath fluctuations couple differently to each of the two levels through interactions $h_g^{(0)}$ and $h_e^{(0)}$ for the ground and excited states, respectively. The bath fluctuations perturb the energies of each of the two levels differently and hence cause fluctuations in the transition energies. If such a fluctuation occurs during the time interval between the first two matter-radiation interactions, that particular two-level system (TLS) will evolve with an altered transition energy with respect to the value at the time of the first interaction with the pulse. Differences in the local solvent structures will also result in differences in the electronic transition energies of the TLSs in the ensemble. If the solvent structure about a TLS is maintained for the timescale of the measurement, i.e., a static energy shift, then the phase evolution of the TLS can be reversed by the photon echo pulse sequence. This results in the rephasing of ensemble coherence.

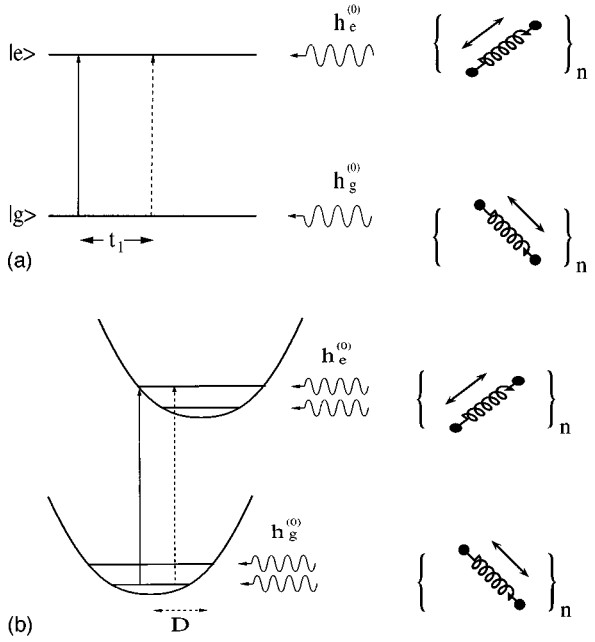

FIG. 1. (a) Model of a two-level system coupled to the bath consisting of a set of oscillators. (b) Model of a multilevel system coupled to the bath.

Figure 1(b) depicts a multi-level chromophore where each vibronic transition in the absorption spectrum has the same couplings (i.e., h_g and h_e) to the bath. Here the width of the simulated absorption spectrum is broadened by these vibronic transitions while the photon echo response will be affected by the high Bohr frequency contributions to the phase evolution of the ensemble. Other complications that arise in the multi-level case include the displacement D of the chromophore equilibrium position between ground and excited electronic states. Furthermore, several intra-chromophore vibrational modes may have vibronic activity and have to be taken into account in the simulation of the nonlinear optical response. These issues will be addressed in the remainder of this section.

A. Photon echo signals and the model of material response function

In the case of two-pulse photon echoes, the time-integrated echo signal detected in the $2k_2-k_1$ phase matching direction is expressed as a function of time delay τ between the two pulses as

$$I(\tau)=\int_{-\infty}^{\infty} dt|P^{(3)}_{2k_2-k_1}(t,\tau)|^2. \tag{1}$$

By contrast, the time-gated photon echo is generated by focusing the photon echo signal and the up-converting pulse into a doubling crystal to generate the second harmonic. The intensity of the second harmonic signal is written as

$$I(t',\tau)=\int_{-\infty}^{\infty} dt|P^{(3)}_{2k_2-k_1}(t,\tau)|^2\times|E(t-t')|^2, \tag{2}$$

where t' reflects the independent time delay of the gate pulse.

Downloaded¬09¬Sep¬2001¬to¬128.135.233.49.¬Redistribution¬subject¬to¬AIP¬license¬or¬copyright,¬see¬http://ojps.aip.org/jcpo/jcpcr.jsp

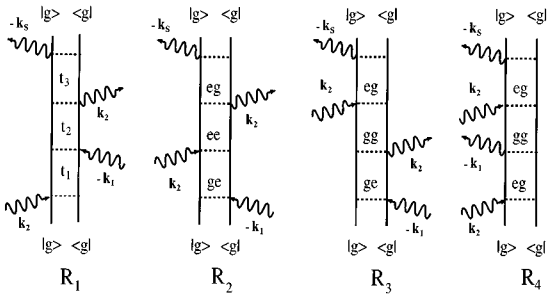

FIG. 2. Feynman diagrams for two-pulse photon echoes. See the text for details.

The third-order polarization in a system with two electronic states and under the rotating wave approximation takes the form[12]

$$
\begin{aligned}
&P^{(3)}_{2k_2-k_1}(t,\tau)\\
&\quad=\int_0^\infty dt_3\int_0^\infty dt_2\int_0^\infty dt_1 e^{-i\Omega(t-2\tau)}\\
&\qquad\times\{(R_1+R_4)e^{-i(\omega_{eg}-\Omega)(t_3+t_1)}\\
&\qquad\times E_2(t-t_3-\tau)E_1^*(t-t_3-t_2)E_2(t-t_3-t_2-t_1-\tau)\\
&\qquad+(R_2+R_3)e^{-i(\omega_{eg}-\Omega)(t_3-t_1)}\\
&\qquad\times E_2(t-t_3-\tau)E_2(t-t_3-t_2-\tau)E_1^*(t-t_3-t_2-t_1)\},
\end{aligned}
\tag{3}
$$

where Ω is the laser center frequency, ω_{eg} is the energy difference between excited ($|e\rangle$) and ground ($|g\rangle$) electronic states at the equilibrium positions, E_i denotes the field amplitude, and R_i represents the material response function.

The non-intuitive form for the response functions can be visualized using double-sided Feynman diagrams, as shown in Fig. 2. The applied fields and interactions with the system (both two-level and multi-level) are depicted by k-vectors k_1 and k_2. The signal field is denoted by k_s satisfying appropriate momentum matching conditions (i.e., $2k_2-k_1$). The time ordering of the interactions occurs with the first interaction at the bottom of the diagram and the signal field at the top. Response functions R_2 and R_3 allow for echo formation through polarization rephasing for positive delay times (i.e., k_1 before k_2) while R_1 and R_4 cannot form a true echo since rephasing is not possible.

The central issue in the calculation of Eq. (3) for a chromophore in solution focuses on modeling the material responses. Here we adopt the Yan and Mukamel model Hamiltonian.[13] The Hamiltonian of a solute-solvent system, H^T, expressed in terms of the solute electronic state representation, is given by

$$
\begin{aligned}
H^T&=|g\rangle[H_g^T(\boldsymbol{Q}_S,\boldsymbol{Q}_B,\boldsymbol{q}_B)]\langle g|\\
&\quad+|e\rangle[H_e^T(\boldsymbol{Q}_S,\boldsymbol{Q}_B,\boldsymbol{q}_B)+\hbar\omega_0]\langle e|\\
&=|g\rangle[H_g(\boldsymbol{Q}_S)+h(\boldsymbol{Q}_B)+H_g'(\boldsymbol{Q}_S,\boldsymbol{Q}_B)+\hbar W_g^{el}]\langle g|\\
&\quad+|e\rangle[H_e(\boldsymbol{Q}_S)+h(\boldsymbol{Q}_B)+H_e'(\boldsymbol{Q}_S,\boldsymbol{Q}_B)+\hbar\overline{W_e^{el}}\\
&\quad+\hbar\omega_0]\langle e|.
\end{aligned}
\tag{4}
$$

Here the nuclear and electronic degrees of freedom of the solvent are denoted by $\boldsymbol{Q}_B$ and $\boldsymbol{q}_B$, respectively, while the nuclear degrees of freedom of the solute are denoted by $\boldsymbol{Q}_S$. The 0-0 transition frequency of the isolated solute is given by ω_0. The ground and excited Hamiltonians of the solute-solvent system, H_g^T and H_e^T, are further partitioned into four parts - the isolated system $(H_m(\boldsymbol{Q}_S), m=e,g)$, the isolated bath $(h(\boldsymbol{Q}_B))$, the coupling between the solute in the $|m\rangle$ electronic state and the nuclear degrees of freedom of the bath $(H_m'(\boldsymbol{Q}_S,\boldsymbol{Q}_B))$, and the coupling between system electronic degrees of freedom and bath electronic degrees of freedom $(\hbar W_m^{el})$. The separation of the coupling energy into $H_m'(\boldsymbol{Q}_S,\boldsymbol{Q}_B)$ and $\hbar W_m^{el}$ results from the assumption that the response time of the bath electrons to a change in the solute electronic state is short compared to any nuclear motions (Bohn–Oppenheimer approximation). The electronic-electronic coupling energy can be further averaged over bath electronic coordinates, $\boldsymbol{q}_B$, resulting in the expectation value $\overline{W_m^{el}}$.

The averaged electronic energy is defined as

$$
\omega_{eg}\equiv\omega_0+\overline{W_e^{el}}-\overline{W_g^{el}},
\tag{5}
$$

and to simplify the notation, $\overline{W_g^{el}}$ is set as the energy origin (i.e., $\overline{W_g^{el}}=0$). The Hamiltonian is then written in the form

$$
H^T=|g\rangle[\hat{H}_g(\boldsymbol{Q}_S,\boldsymbol{Q}_B)]\langle g|+|e\rangle[\hat{H}_e(\boldsymbol{Q}_S,\boldsymbol{Q}_B)+\hbar\omega_{eg}]\langle e|,
\tag{6}
$$

with

$$
\hat{H}_g(\boldsymbol{Q}_S,\boldsymbol{Q}_B)=H_g(\boldsymbol{Q}_S)+h(\boldsymbol{Q}_B)+H_g'(\boldsymbol{Q}_S,\boldsymbol{Q}_B),
\tag{7}
$$

$$
\hat{H}_e(\boldsymbol{Q}_S,\boldsymbol{Q}_B)=H_e(\boldsymbol{Q}_S)+h(\boldsymbol{Q}_B)+H_e'(\boldsymbol{Q}_S,\boldsymbol{Q}_B).
\tag{8}
$$

The energy gap between the two electronic states along the nuclear coordinates is defined using Eq. (6) as[13]

$$
\begin{aligned}
U&\equiv\hat{H}_e(\boldsymbol{Q}_S,\boldsymbol{Q}_B)-\hat{H}_g(\boldsymbol{Q}_S,\boldsymbol{Q}_B)\\
&=[H_e(\boldsymbol{Q}_S)-H_g(\boldsymbol{Q}_S)]+[H_e'(\boldsymbol{Q}_S,\boldsymbol{Q}_B)-H_g'(\boldsymbol{Q}_S,\boldsymbol{Q}_B)]\\
&\equiv\Delta H(\boldsymbol{Q}_S)+\Delta H'(\boldsymbol{Q}_S,\boldsymbol{Q}_B).
\end{aligned}
\tag{9}
$$

Here ΔH is defined as the difference between the excited and ground state Hamiltonians of the isolated system and $\Delta H'$ as the difference of the coupling Hamiltonians.

The linebroadening function $g(t)$, which is a building block for all linear and nonlinear material response functions, can be written in terms of the average of U and its correlation function[12,13]

$$
g(t)=i\lambda t+\int_0^t d\tau_1\int_0^{\tau_1} d\tau_2\ddot{g}(\tau_2),
\tag{10}
$$

$$
\lambda=\langle U\rangle,
\tag{11}
$$

Downloaded¬09¬Sep¬2001¬to¬128.135.233.49. Redistribution subject to AIP license or copyright,¬see¬http://ojps.aip.org/jcpo/jcpcr.jsp

$$\ddot{g}(t)=\langle U(t)U\rangle-\langle U\rangle^2, \tag{12}$$

$$U(t)\equiv\exp(i\hat{H}_g t)U\exp(-i\hat{H}_g t). \tag{13}$$

The correlation function $\langle U(t)U\rangle$ is governed by the system nuclear motions [i.e., $H_m(\boldsymbol{Q}_S)$] and the couplings between the system and solvent nuclear coordinates [i.e., $H'_m(\boldsymbol{Q}_S,\boldsymbol{Q}_B)$]. In the case that both electronic states are bound and the nuclear degrees of freedom of the system only undergo relatively small amplitude motions, $H'_m(\boldsymbol{Q}_S,\boldsymbol{Q}_B)$ may be expanded around the equilibrium configuration of the system, resulting in

$$H'_m(\boldsymbol{Q}_S,\boldsymbol{Q}_B)=h_m^{(0)}(\boldsymbol{Q}_B,\boldsymbol{Q}_S^0)+\sum_{n=1}^{\infty}h_m^{(n)}(\boldsymbol{Q}_B)(\boldsymbol{Q}_S-\boldsymbol{Q}_S^0)^n$$
$$\equiv h_m^{(0)}(\boldsymbol{Q}_B)+V'_m(\boldsymbol{Q}_S,\boldsymbol{Q}_B). \tag{14}$$

Here $h_m^{(0)}(\boldsymbol{Q}_B)$, evaluated at the solute equilibrium position, reflects the direct coupling of the bath nuclear motions to the solute electronic degrees of freedom and plays an important role in the electronic dephasing. $V'_m(\boldsymbol{Q}_S,\boldsymbol{Q}_B)$, the sum of the higher-order terms of the Taylor expansion, represents the interaction between the bath nuclear motion and the system nuclear motion. This interaction induces vibrational and rotational dephasing and relaxation. In general, vibrational and rotational dephasing occurs much slower than electronic dephasing. Hence, in the treatment of photon echo signals, we neglect the $V'_m(\boldsymbol{Q}_S,\boldsymbol{Q}_B)$ and only focus on $h_m^{(0)}(\boldsymbol{Q}_B)$.

We consider an intuitively simple case where the bath consists of a set of harmonic oscillators representing the solvent instantaneous[24–26] or optimal[27] normal modes and the solute electronic states couple linearly to the bath coordinates,[28–30] that is,

$$h_m^{(0)}(\boldsymbol{Q}_B)=\sum_i c_m^i Q_B^i, \tag{15}$$

where the summation spans the bath normal modes. This is a good approximation for the induced dipole interactions where the interaction energy is linearly proportional to the solvent polarizability. The first nontrivial term in the Taylor expansion of solvent polarizability relative to the solvent nuclear coordinate is the linear term.

The electronic Hamiltonian, $\hat{H}_m$, defined in Eq. (8) in the present case contains only orthogonal terms with respect to $\boldsymbol{Q}_S$ and $\boldsymbol{Q}_B$. Therefore, the correlation function $\langle U(t)U\rangle$ becomes

$$\langle U(t)U\rangle=\langle\Delta H(\boldsymbol{Q}_S,t)\Delta H(\boldsymbol{Q}_S,0)\rangle$$
$$+\langle\Delta h^{(0)}(\boldsymbol{Q}_B,t)\Delta h^{(0)}(\boldsymbol{Q}_B,0)\rangle$$
$$=\langle\Delta H(\boldsymbol{Q}_S,t)\Delta H(\boldsymbol{Q}_S,0)\rangle$$
$$+\sum_i(\delta c^i)^2\langle Q_B^i(t)Q_B^i(0)\rangle, \tag{16}$$

where

$$\Delta H(\boldsymbol{Q}_S,t)=\exp(iH_g t)\Delta H(\boldsymbol{Q}_S)\exp(-iH_g t), \tag{17}$$

$$Q_B^i(t)=\exp[i(h^i+h_g^{(0)i})t]Q_B^i\exp[-i(h^i+h_g^{(0)i})t], \tag{18}$$

and

$$\delta c^i\equiv c_e^i-c_g^i. \tag{19}$$

The first term on the right hand side of Eq. (16) is the contribution from the system modes which have Franck-Condon progressions along the optical transition (i.e., $H_e\neq H_g$). If the excitation involves preparation of one or more vibrational coherences, quantum beats[31–33] may be observed in the echo signal[21] provided that electronic dephasing is slower than the recurrence of the quantum beats. In this case the quantum beat decay envelope would reflect the electronic dephasing time. On the other hand, if the electronic dephasing time is shorter than the recurrence of quantum beats, the decay of the observed echo may be influenced by phase interference between oscillations instead of phase interruption by the interactions with the environment. The second term on the r.h.s. of Eq. (16) is due to the coupling to bath nuclear motions. As mentioned in the Introduction, the OKE response can provide information about solvent nuclear motions that affect the optical dynamics.[16,34] The solvent OKE signal and the chromophore pump-probe spectrum and their connection and contribution to the photon echo response are examined in the next two sections.

Finally, the linebroadening functions are used in evaluating the response function for the echo calculation. The echo response functions, evaluated using cumulant expansions to second order, have the forms[13]

$$R_1=\exp\{-g^*(t_3)-g(t_1)-f_+(t_3,t_2,t_1)\}, \tag{20}$$

$$R_2=\exp\{-g^*(t_3)-g^*(t_1)+f_+^*(t_3,t_2,t_1)\}, \tag{21}$$

$$R_3=\exp\{-g(t_3)-g^*(t_1)+f_-^*(t_3,t_2,t_1)\}, \tag{22}$$

$$R_4=\exp\{-g(t_3)-g(t_1)-f_-(t_3,t_2,t_1)\}, \tag{23}$$

where

$$f_+(t_3,t_2,t_1)=g^*(t_2)-g^*(t_2+t_3)$$
$$-g(t_1+t_2)+g(t_1+t_2+t_3), \tag{24}$$

$$f_-(t_3,t_2,t_1)=g(t_2)-g(t_2+t_3)$$
$$-g(t_1+t_2)+g(t_1+t_2+t_3). \tag{25}$$

The linear absorption cross section can be calculated according to[35]

$$\sigma_A(\omega)=2\omega\times Re\int_0^{\infty}\exp\{-g(t)\}\exp\{-i(\omega-\omega_{eg})t\}dt. \tag{26}$$

B. The relation between OKE and solvent-induced electronic dephasing

A principle objective of this paper is the rigorous evaluation of the linebroadening, hence response, functions using independently measured experimental information about solvent fluctuations. The OKE is a measure of the optically induced anisotropic polarizability response of a sample (i.e., off-resonant birefringence). The tensor element of the OKE response function of a pure solvent, written in terms of rotational motions and intramolecular and intermolecular vibrational coordinates (Q_j), is given by[36]

Downloaded 09 Sep 2001 to 128.135.233.49. Redistribution subject to AIP license or copyright, see http://ojps.aip.org/jcpo/jcpcr.jsp

$$\chi^{(3)}_{abcd}(t) \equiv Y^R_0(t) + \sum_j \left[\frac{\partial \alpha_{ab}}{\partial Q_j} \otimes \frac{\partial \alpha_{cd}}{\partial Q_j} \right] \times \left\langle \frac{i}{\hbar} (Q_j(t) Q_j(0) - Q_j(0) Q_j(t)) \right\rangle, \quad (27)$$

where

$$Q_j(t) = \exp[ih^j t] Q_j \exp[-ih^j t]. \quad (28)$$

The OKE signal reflects the difference of two tensor elements,[36]

$$\chi^{(3)}_{OKE}(t) = \chi^{(3)}_{ZZZZ}(t) - \chi^{(3)}_{YYZZ}(t). \quad (29)$$

The first term on the r.h.s. of Eq. (27) is the correlation function of molecular orientations. The molecular orientational motions for simple liquids occur on a picosecond time scale. These motions usually cause a static environmental distribution on the femtosecond two-pulse photon echo timescale and are partially responsible for spectral diffusion on timescales accessible to three-pulse photon echo measurements.[23]

A comparison of Eq. (29), Eq. (27), and Eq. (16) suggests that the OKE response may describe the solvent-induced electronic energy fluctuations under the following conditions: (1) The solvent-induced electronic energy fluctuations result from the coupling to the solvent nuclear modes that modulate the solvent polarizability (i.e., $\partial\alpha/\partial Q_j \neq 0$); (2) only the anisotropic part of the solvent polarizability modulates the chromophore electronic energy ($\chi^{(3)}_{ZZZZ} - \chi^{(3)}_{YYZZ} \neq 0$); (3) the ground and excited state coupling constants are different (i.e., $\delta c^i \neq 0$); (4) the coupling constants c^i_g and c^i_e are linearly proportional to the first derivative of the solvent polarizability with respect to the nuclear coordinates, such that

$$(\delta c^i)^2 = N^i \left\langle \frac{\partial \alpha_{ZZ}}{\partial Q^i_B} \otimes \frac{\partial \alpha_{ZZ}}{\partial Q^i_B} - \frac{\partial \alpha_{YY}}{\partial Q^i_B} \otimes \frac{\partial \alpha_{ZZ}}{\partial Q^i_B} \right\rangle, \quad (30)$$

where N^i is a proportionality constant; (5) the solute-solvent interaction, $h^{(0)}_g$, is small compared to the pure solvent energy h^i - the evolution of $Q^i_B(t)$ is then mainly governed by h^i. In other words, the change of the solvent dynamics due to the presence of the solute can be neglected on the time scale of electronic dephasing.

For a molecule with a small dipole moment and for a small or no change in the magnitude of this dipole upon optical excitation, as in the cyanine dyes HDITC and HITCI, the coupling between solute and solvent occurs mainly through weak induced-dipole interactions.[16] The aforementioned conditions for the solvent-solute interactions may be satisfied for this class of chromophores. Thus the OKE response of the pure solvent will closely reflect the spectral density of solvent-induced electronic energy fluctuation, $C_{PE}(\omega)$, which is defined as the Fourier transform of the correlation function $\langle \Delta h^{(0)}(\boldsymbol{Q}_B, t) \Delta h^{(0)}(\boldsymbol{Q}_B, 0) \rangle$. This spectral density can be derived using the fluctuation-dissipation theorem[12] and the assumptions of the two previous paragraphs as

$$C_{PE}(\omega) \equiv \int_{-\infty}^{\infty} dt \langle \Delta h^{(0)}(\boldsymbol{Q}_B, t) \Delta h^{(0)}(\boldsymbol{Q}_B, 0) \rangle e^{i\omega t} = N(\omega) \left[1 + \coth\left(\frac{\hbar\omega}{2k_B T} \right) \right] Im[\chi^{(3)}_{OKE}(\omega)]. \quad (31)$$

Here we simply assume that N^i in Eq. (30) depends only on frequency but not on the particular type of mode. Using the spectral density of the solute solvent coupling, the solvent-induced linebroadening function, $g_B(t)$,[12] is given by

$$g_B(t) = \frac{1}{2\pi} \int_{-\infty}^{\infty} d\omega \frac{1 - \cos(\omega t)}{\omega^2} C(\omega) + \frac{i}{2\pi} \int_{-\infty}^{\infty} d\omega \frac{\sin(\omega t) - \omega t}{\omega^2} C(\omega) + i\lambda t. \quad (32)$$

This, along with Eq. (31), describes the bath contribution to the optical dephasing spectral density and linebroadening function.

C. Wavepacket picture of pump-probe spectroscopy

The frequencies of oscillatory components observed in a pump-probe experiment and the Fourier spectrum give the underdamped vibrational frequencies involved in the optical excitation. The relative amplitudes and absolute phase angles of the oscillatory components in regular (i.e., wavelength integrated) and wavelength-resolved pump-probe spectra are used to assign the contributions of vibrational modes in the excited and ground electronic states of the chromophore. The theoretical background for this assignment can be visualized using the wavepacket picture.[37,38] A brief discussion of the wavepacket picture of pump-probe spectroscopy is given in the following. The detailed results of calculations of phase angles and amplitudes will be shown elsewhere.[39]

The Feynman diagrams for the pump-probe processes in the two potential surfaces are similar to those given in Fig. 2, but are obtained by replacing first k_2 (from the bottom of the figure) with k_1 and k_s with k_2. The evolution of a pump-probe process can be described by the independent propagations of bra and ket vectors on either the ground or excited potential surfaces in three time intervals, t_3, t_2, and t_1. The pump and probe pulse durations determine the range of t_1 and t_3, respectively. The range of t_2 is bound by the time delay (defined as τ') between pump and probe plus/minus the pulse durations. The intensity of the signal is interpreted as the time-dependent overlap of the final bra and ket vectors. During t_2, both bra and ket vectors for the processes resulting in stimulated emission (i.e., R_1 and R_2) propagate on the excited electronic state. These two processes reflect the excited state vibrational dynamics in the pump-probe spectrum. By contrast, the bra and ket vectors in the resonant impulsive Raman (R_3) and the hole burning (R_4) processes move on the ground state potential surface during t_2. The ground state dynamics are, therefore, projected out by these latter two processes.

When using pulses of 20 fs duration, the wavepacket propagation picture[37,38] suggests that the amplitudes of the oscillations observed in stimulated emission are stronger than the respective ground state contribution for those under-

Downloaded 09 Sep 2001 to 128.135.233.49. Redistribution subject to AIP license or copyright, see http://ojps.aip.org/jcpo/jcpcr.jsp

damped modes with vibrational frequencies less than about 500 cm^{-1}. This is because the ground state vibrational wavepacket prepared by two interactions with the pump pulse does not develop much momentum in the excited electronic state before it is dumped back to the ground state. The propagation of a wavepacket in the ground state during time delay τ' is then confined to a small region of the coordinate. The change of the final nonstationary ket and bra vector overlap with time delay is therefore small. By contrast, the excited state wavepacket probed by stimulated emission propagates comparatively large distances during τ'. The amplitude of the oscillation observed in stimulated emission is relatively large. If the frequency of a vibrational mode changes from the ground state to the excited state, one should observe stronger oscillations associated with the excited state frequencies than with ground state frequencies provided that the excited state vibrational dephasing time is long compared to the vibrational period.

The absolute phase angles of the oscillatory components are determined by the assumption that the signal can be represented by a sum of exponentially damped cosinusoidal functions,

$$S_{PP}(\tau')=\sum_i A_i\cos(\omega_i\tau'+\phi_i)\exp(-\gamma_i\tau'). \tag{33}$$

The wavepacket picture indicates that the initial phase angle, ϕ_i, of an oscillatory component in a wavelength-resolved pump-probe spectrum is determined by the average distances that bra and ket wavepackets propagate along the respective potential surfaces during t_1 and t_3. The average distances are, in turn, determined in a complicated way by the pulse duration, electronic dephasing, potential displacement, and laser detuning.[40,41] The bra and ket wavepackets in the four pump-probe pathways propagate with different time orderings on different potential surfaces during t_3 and t_1, resulting in different phase angles. Therefore a measured phase angle can be an indicator about the processes which contribute to the oscillations.[39]

D. The effect of chromophore intramolecular vibrational modes

The linebroadening functions corresponding to solute vibrational motions are evaluated using the analyzed pump-probe response. It was argued above that the chromophore vibrational motions can be treated as isolated oscillators on the time scale of electronic dephasing. The simplest case, also the case for HITCI and HDITC (see the result below), is an isolated harmonic vibrational mode with frequency ω_i for both the ground and excited electronic states with potential displacement D_i. The electronic energy difference along the nuclear coordinate, $\Delta H(Q_S)$, is given by

$$\Delta H(Q_S)=\hbar\omega_i D_i\left(Q_S+\frac{D_i}{2}\right). \tag{34}$$

The average of this energy difference, which equals half the measured steady-state Stokes-shift due to vibrational relaxation along this coordinate, is[13]

$$\lambda_v^i=\langle\Delta H(Q_S)\rangle=\frac{\hbar\omega_i D_i^2}{2}. \tag{35}$$

The energy correlation function is given by

$$\langle\Delta H(Q_S,t)\Delta H(Q_S,0)\rangle = \frac{(\hbar\omega_i D_i)^2}{2}[e^{i\omega_i t}\bar{m}+e^{-i\omega_i t}(\bar{m}+1)], \tag{36}$$

where $\bar{m}$ is the Bose factor $\bar{m}=\{\exp(\hbar\omega/kT)-1\}^{-1}$.

Using Eq. (35) and Eq. (36), the linebroadening function, $g_v(t)$, for each optically active vibrational mode becomes

$$g_v^i(t)=D_i^2\{\bar{m}(1-\cos(\omega_i t))-0.5(\exp(-i\omega_i t)-1)\}. \tag{37}$$

Oscillatory terms in the linebroadening function arise from vibrational coherence (i.e., impulsive) excitation. The magnitude of this oscillation is dictated by the displacement D_i. For a solute with multiple vibrational modes, the final linebroadening function is taken to be the superposition

$$g_v(t)=\sum_i g_v^i(t). \tag{38}$$

The resulting superposition of oscillatory responses of incommensurate frequency modes can contribute to the decay of the measured optical coherence. The total linebroadening fuction used in simulation of photon echo signals and absorption spectra is the sum of Eqs. (32) and (38).

III. EXPERIMENT

The experimental apparatus has been described in greater detail elsewhere.[9,16,33] The laser system used for the echo measurements and the k-vector diagram of the experiment are the same as in Ref. 9. The short pulse source is a home-built Kerr lens modelocked Ti Sapphire laser[42,43] that is of a unique cavity-dumped design and capable of producing 12–15 fs duration transform limited Gaussian pulses with 80–100 nm spectral bandwidth.[44] Non-cavity dumped and cavity-dumped pulses are used for the data reported here. The 84 MHz or 100 kHz train of pulses is split into two beams with k-vectors k_1 and k_2 and an intensity ratio of 1:2, and are focused into a flowing dye jet of the chromophores HITCI or HDITC in DMSO. The optical density of the jet at the absorption center wavelength of the dyes is maintained at 0.3 or less. Pulse energies at the sample are 1–2 nJ. The diffracted photon echo signals in the $2k_2-k_1$ and $2k_1-k_2$ directions are detected with photomultipliers (Hamamatsu R928) or with a photodiode/preamp detector (Centronic), processed with a digital lock-in amplifier (SRS-850), and recorded for each 2 fs increment of a stepper delay line. The OKE data are obtained using non-cavity dumped pulses from a Ti-Sapphire laser that are 20 fs in duration and have 60 nm spectral bandwidth.

IV. EXPERIMENTAL AND NUMERICAL RESULTS

The numerical calculations involve evaluating Eq. (3) and require several types of input. The paradigm being de-

Downloaded¬09¬Sep¬2001¬to¬128.135.233.49. Redistribution subject to AIP license or copyright,¬see¬http://ojps.aip.org/jcpo/jcpcr.jsp

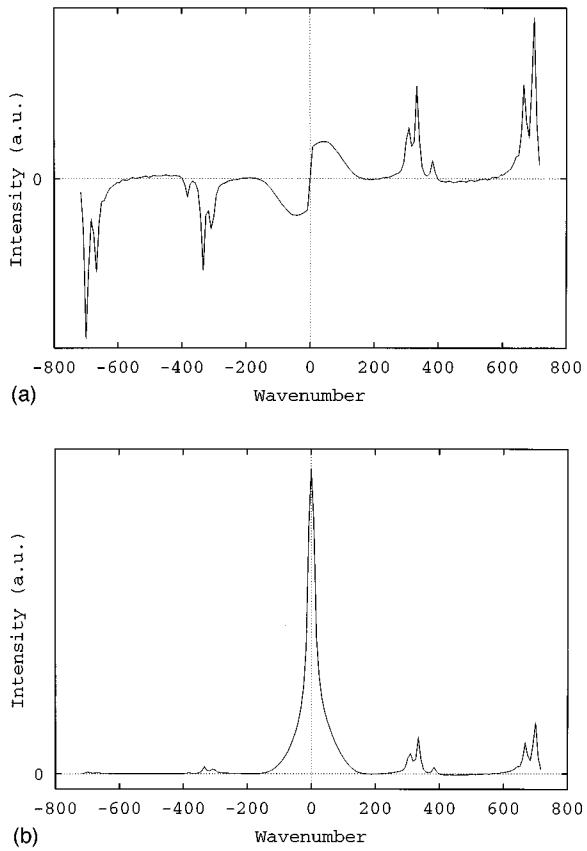

FIG. 3. (a) The OKE susceptibility of DMSO. (b) Polarizability spectral density of DMSO.

scribed in this paper is the use of the OKE spectrum as the spectrum of solvent fluctuations that result in optical dephasing. A second consideration involves estimating how much of the spectral evolution between absorption and emission steady-state spectra involves solvation or vibrational relaxation processes. Finally, the intra-chromophore modes that are coupled to the optical excitation coordinate must be taken into account.

The Stokes-shift of HITCI and HDITC in a range of solutions exhibit almost no solvent dependence.[16,33] It is, therefore, assumed that most of the Stokes-shift is due to vibrational relaxation; the solvent-induced Stokes-shift is set equal to zero. As long as the ground and excited state coupling constants are different [e.g., a condition (3) of Eq. (30)] the electronic energy difference is modulated. By contrast, the solution coordinate in a conventional Brownian oscillator is assumed to be a displaced oscillator; both ground and excited states have the same oscillator frequency. In this case a displacement is necessary for modulation of the energy difference (i.e., $D_i \neq 0$; therefore $\lambda \neq 0$). Our model with $\lambda = 0$ can be thought of as a Brownian oscillator with different frequencies in the two states but without a displacement.

A. OKE spectral density

Figure 3(a) shows the imaginary part of the OKE susceptibility, $\mathrm{Im}[\chi^{(3)}(\omega)]$, of DMSO that is measurable with a 60 nm laser spectral bandwidth. The frequencies of intramolecular vibrational modes are in good agreement with the Raman spectrum,[45] while the relative intensities of the OKE to the Raman spectra reflect the anisotropy of each mode. The step size in the experimental OKE susceptibility is about 8 cm^{-1}. The polarizability spectral density, $C(\omega)$, of DMSO is shown in Fig. 3(b) and is calculated from the data of Fig. 3(a) using Eq. (31). The intensities of negative frequencies relative to those of positive frequencies in Fig. 3(b) satisfy detailed balance [see Eq. (31)]. Since the experimental data do not provide enough resolution to accurately describe the asymptotic behavior of $C(\omega)$ as $\omega \rightarrow 0$, the determination of $C(\omega=0)$ is somewhat arbitrary. However, as shown below, the simulated two-pulse echo signals are insensitive to the intensity of $C(\omega \leqslant 8\ \mathrm{cm}^{-1})$.[46] The intensity of $C(\omega)$ near $\omega=0$ in Fig. 3(b) is calculated by the interpolation routine, polint,[47] with 5 data points around $\omega=0$ (3 points at $\omega>0$ and two points at $\omega<0$).

B. Two-level system coupled to solvent bath

Numerical results that assume only solvent-induced electronic fluctuations are considered before including chromophore vibrations. Echo signals are calculated using the polarizability spectral density of the pure solvent to examine how well the spectral density alone can be used to fit the experimental data. Cho *et al.*[36] and Vöhringer *et al.*[16] had employed the spectral density of solvent intermolecular modes to model solvation and solvent-induced dephasing via energy fluctuations, respectively. The present numerical results are more accurate than those presented in Ref. 16 due to the more rigorous treatment of the finite pulse durations and the inclusion of all four response functions $R_1 - R_4$ rather than just R_2 and R_3

The calculation of the echo signals was performed using two different integration routines.[48] The three-fold integrals of Eq. (3) were calculated using a Monte Carlo integration routine (i.e., vegas).[47] The real and imaginary parts of $P^{(3)}$ were integrated separately. The precision was set at 2% of the iterative calculated values. The integration over time t in Eq. (1) was performed by the Romberg integration method.[47] The precision is set at 1%.

Figure 4 shows the overlay of the experimental echo signal from HITCI in DMSO and the signals calculated using the intermolecular part of the DMSO spectral density [the intensity between $\pm$ 163 cm^{-1} in Fig. 3(b)] with different values for the solvent-solute coupling parameter, N. Here we simply assume that N is frequency-independent. As N increases the peak shift and the width of the calculated echo decrease. Physically, increasing N increases the amplitude of the electronic energy fluctuations, and therefore accelerates electronic dephasing. For a value of $N=3.4$, the width of the calculated echo signal is smaller than the experimental signal but the shift is still larger than the experimental one (18 fs vs 15 fs). Increasing N will eventually cause the shift to decrease to 15 fs but the width of the calculated echo will become even narrower. This indicates that solvent intermolecular (i.e., collective) vibrational motions are not sufficient to fully account for the observed electronic energy fluctuations. Simulations using a frequency dependent coupling,

Downloaded¬09¬Sep¬2001¬to¬128.135.233.49.¬Redistribution¬subject¬to¬AIP¬license¬or¬copyright,¬see¬http://ojps.aip.org/jcpo/jcpcr.jsp

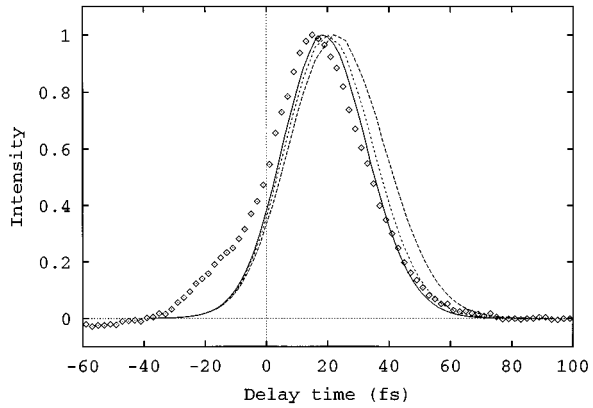

FIG. 4. Experimental and calculated two-pulse photon echo signals of HITCI in DMSO. The calculated signals are obtained using a two-level system coupled to the intermolecular part of the polarizability spectral density of DMSO. Diamond: experimental data; long dashed line: $N=1.4$; short dashed line: $N=2.4$; solid line: $N=3.4$. The sech^2 pulse duration of 17 fs was chosen to reproduce the experimental response function.

$N(\omega)$, have not been performed to test the uniqueness of this conclusion.

Figure 5 displays calculated echoes using different ranges of solvent spectral density with the same coupling parameter $N=1.4$. The calculated time shift and width of the echo signal decrease significantly when the frequency range of the spectral density used increases from ± 163 to ± 391 cm^{-1}; the latter range includes the first set of solvent intramolecular modes. By contrast, the width and shift only change slightly when the range increases to include the other three intramolecular modes around 700 cm^{-1} (see Fig. 3). The echo signal that is calculated using the full frequency range of the measured spectral density fits the experimental signal very well at positive time delay but deviates from experiment at negative delays. The ''lump'' in the experimental signal at the negative time is actually due to a thermal effect caused by the high repetition rate (84 MHz not cavity-dumped) pulse train interrogating the sample.[16] The intensity of this lump deceases when the sample flow rate increases or the pulse repetition rate decreases. The result shown here supports the conclusion drawn by the comparison in Fig. 4 that the solvent intramolecular modes play an essential role in shaping the two-pulse photon echo.

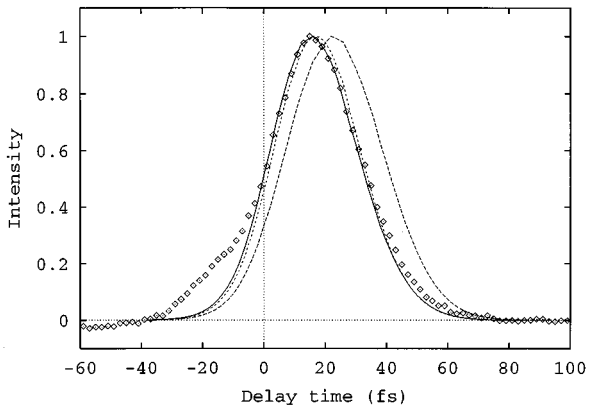

FIG. 5. Experimental and calculated two-pulse photon echo signals of HITCI in DMSO. The calculated signals are obtained using a two-level system coupled to different ranges of the polarizability spectral density of DMSO with the same coupling parameter of $N=1.4$. Diamond: experimental data; long dashed line: $C(|\omega|< 163\ \mathrm{cm}^{-1})$; short dashed line: $C(|\omega|< 391\ \mathrm{cm}^{-1})$; solid line: $C(|\omega|< 716\ \mathrm{cm}^{-1})$. Same pulse duration as Fig. 4.

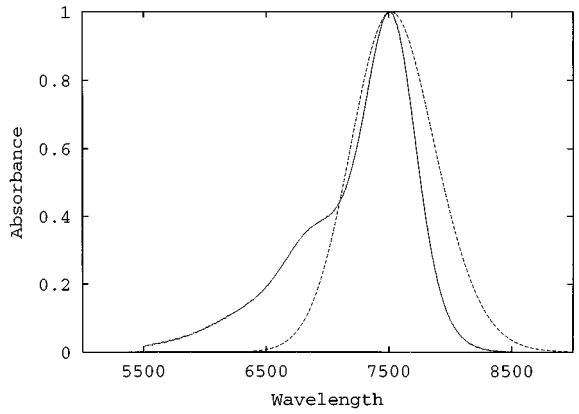

FIG. 6. Experimental and calculated absorption spectra of HITCI in DMSO. Solid line: experimental data; dashed line: calculated data using a two-level system coupled to the full range of experimental polarizability spectral density of DMSO and $N=1.4$.

The linear absorption spectrum is calculated and compared to the experimental one in Fig. 6 using the full range of the measured spectral density of DMSO shown in Fig. 3(b) and using a value for the coupling parameter of $N=1.4$. Although the same set of parameters give a good fit to the echo signal, the calculated absorption spectrum is much broader than the experimental main peak. This result indicates that fitting the experimental two-pulse echo signal by solvent-induced broadening alone overestimates the solvent-solute interactions. The contributions from chromophore intramolecular modes should be taken into account.

C. Intra-chromophore vibrational modes

Figure 7 shows the pump-probe spectrum of HITCI in decanol and its Fourier transform (i.e., square-root of the power spectrum). The major components in the Fourier spec-

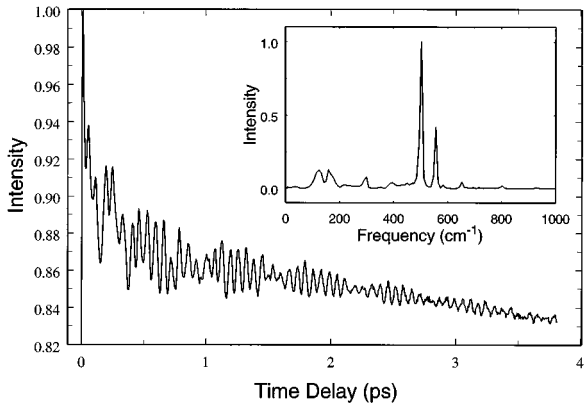

FIG. 7. Wavelength-integrated pump-probe spectrum of HICTI in n-decanol and its Fourier transform.

Downloaded¬09¬Sep¬2001¬to¬128.135.233.49. Redistribution subject to AIP license or copyright,¬see¬http://ojps.aip.org/jcpo/jcpcr.jsp

trum occur at 550, 500, 130, and 160 cm^{-1}; these are assumed to be fundamental mode frequencies. The postresonant Raman spectrum shows three strong ground state modes at 550, 496, and 502 cm^{-1}.[49] The intensity of the 500 cm^{-1} mode in the Fourier spectrum in Fig. 7 is almost twice as large as that of 550 cm^{-1} mode. This is probably due to the overlap of unresolved 502 and 496 cm^{-1} modes. It is assumed that each of these two modes contributes to half of the intensity of the observed feature.

The assignment of the oscillatory components in the pump-probe spectrum to excited and/or ground state contributions is accomplished by addressing the following questions: (1) Do the vibrational frequencies of three strong Raman modes (i.e., 550, 502, 496 cm^{-1}) change in the excited electronic state? (2) If the frequencies change, will the oscillations with excited state frequencies be apparent in the pump-probe spectrum? The background discussion on the wavepacket picture of pump-probe spectroscopy presented in the theoretical section provides a perspective for answering these questions.

The singular value decomposition analysis[33] of the data shown in Fig. 7 indicates that the amplitudes of the low frequency components are smaller than those of the three high frequency modes. There is no reason to believe from our studies[16,33] and to our knowledge no suggestion made in the literature that the excited state vibrational dephasing times of HITCI are short compared to the ground state vibrations. These two conditions imply that the low frequency modes are not the excited state analogs of any high frequency ground state modes. Rather, it appears that the vibrational frequency change of all of the observed vibrational modes is small. For all subsequent calculations, it is assumed that all vibrational modes have the same frequencies in both ground and excited states.

The experimental Stokes-shift sets a limit on the sum of the potential displacements along each vibrational coordinate. The high frequency shoulder in the HITCI absorption spectrum was assigned to the vibronic transition associated with the 1300 cm^{-1} C-C backbone mode.[50] The intensity of this shoulder indicates that the dimensionless displacement along this mode is at least 0.3. Including this mode, the total Stokes-shift of $\sim$400 cm^{-1} sets a limit on the possible displacements for the 492, 502, and 550 cm^{-1} modes of about 0.3. The theoretical initial phase angles of the oscillations in the wavelength-resolved pump-probe spectrum are obtained using singular value decomposition of $P^{(3)}(\omega)$ calculated by the wavepacket propagation formalism[37,51] and the aforementioned frequency and displacement parameters. The calculated and experimental results are given in Table I. The good agreement between two sets of data provides self consistency to the assumptions that optically active vibrational modes can be described by displaced harmonic oscillators and the steady-state Stokes-shift mainly stems from intrachromophore vibrational relaxation as opposed to solvation. Also, the relative amplitudes of the 550 to 500 cm^{-1} features are similar to those in the pump-probe spectrum, provided that the intensity at 500 cm^{-1} has equal contributions from 502 and 492 cm^{-1} modes. The calculation of the phase angles of the two low frequency modes is complicated by the thermal population of higher vibrational states in each vibrational manifold resulting in hot-band transitions. The two low frequency modes are assumed to be displaced harmonic oscillators with displacements of 0.5 for each. The displacements are chosen to fit both the vibrational modulation in the pump-probe spectra and the width of the absorption spectrum.

TABLE I. Experimental and calculated phase angles of the oscillations in frequency-resolved pump-probe measurements of HITCI in n-decanol. Numbers in parenthesis are calculated phase angles. The parameters used for the calculation of phase angles are the potential displacement 0.3; electronic 0-0 transition energy 13300 cm^{-1}; the laser center frequency 12900 cm^{-1}; the laser pulse duration of 20 fs (FWHM of a Gaussian pulse); homogeneous electronic dephasing time 100 fs; Gaussian inhomogeneous distribution 800 cm^{-1} (FWHM). The homogeneous and inhomogeneous widths are chosen by fitting the absorption spectrum.

λ/nm	500 cm^{-1}	550 cm^{-1}
720	11 (31)	32 (11)
730	87 (53)	86 (45)
740	118 (97)	105 (104)
750	161 (143)	169 (140)

D. Consideration of intra-chromophore modes

When the intra-chromophore vibrational modes are included in the simulation as described in the previous section, the magnitude of the solvent-solute coupling parameter is chosen by fitting the absorption spectrum. Figure 8(a) shows the overlay of the experimental absorption spectrum of HITCI/DMSO and the spectra calculated using five intramolecular modes, i.e., 550, 500, 500, 130, and 160 cm^{-1}, with the displacements given in the figure caption. The four curves represent four different ranges of spectral densities with different values of the coupling parameter N. The calculated spectrum only fits the main peak because intrachromophore modes with frequency much higher than 550 cm^{-1} (i.e., 1200 cm^{-1}) are not impulsively excited and therefore are not explicitly considered. The higher energy shoulder observed at 670 nm results from a C-C chain mode of 1300 cm^{-1} frequency discussed in the previous section.

Figure 8(b) depicts the calculated echo signals corresponding to each simulated absorption spectrum shown in Fig. 8(a). The echo response that results in the absence of solvent contributions is completely different than the other curves that include the solvent contribution; it shows a smaller shift and longer decay. By contrast, the large shifts displayed in the other curves that include the solvent contribution indicate that the solvent molecules provide a wide range of slow modulations (inhomogeneous environmental distributions) while the fast decays partially reflect the solvent-induced fast modulations. The calculated echo obtained using only solvent intermolecular modes displays a significantly broader echo width and larger peak shift than seen in experiment. This suggests that the polarizability spectral density associated with low frequency solvent intermolecular modes cannot describe the fast modulation reflected in the measured two-pulse photon echo response. The other two curves fit the experimental data reasonably well.

Downloaded¬09¬Sep¬2001¬to¬128.135.233.49. Redistribution subject to AIP license or copyright, see http://ojps.aip.org/jcpo/jcpcr.jsp

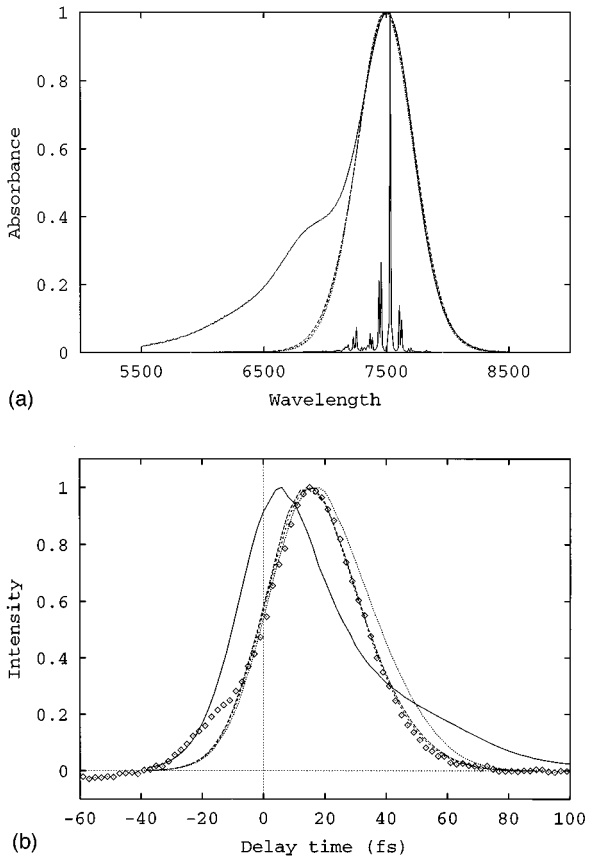

FIG. 8. (a) Experimental and calculated absorption spectra of HITCI in DMSO. (b) Experimental and calculated two-pulse photon echo signals. Five chromophore vibrational modes are used in the calculations. The frequencies and displacements of five vibrational modes are 550 cm^{-1}, 0.3; 500 cm^{-1}, 0.3; 500 cm^{-1}, 0.3; 160 cm^{-1}, 0.5; 130 cm^{-1}, 0.5. (a) Solid line: experimental data; solid structured line: isolated molecule spectrum; a finite linewidth is added for illustration purposes. (b) Diamonds: experimental data; solid line: isolated molecule photon echo signal. (Both panels) Dotted line: ⋯ (as before).

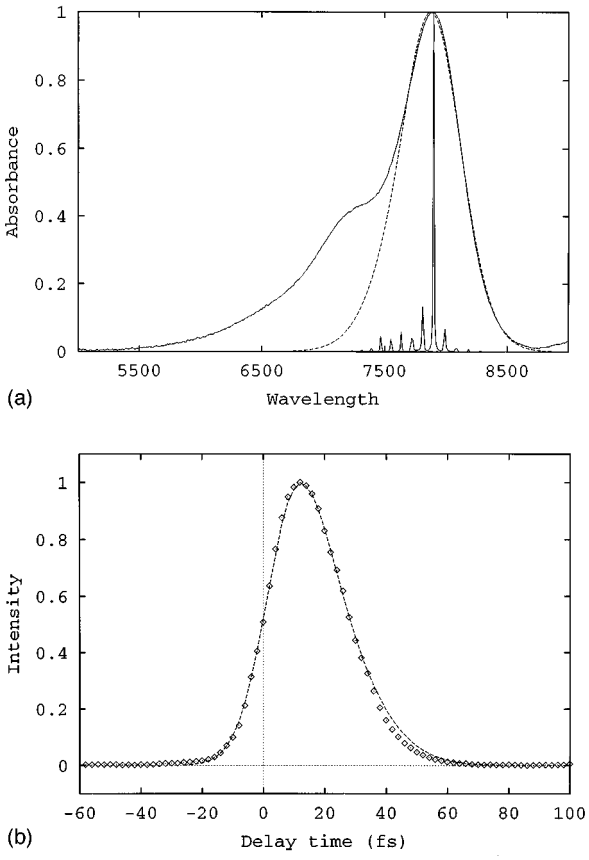

FIG. 9. (a) Experimental and calculated absorption spectra of HITCI in DMSO. (b) Experimental and calculated two-pulse photon echo signals. Five chromophore vibrational modes are used in the calculations. The frequencies and discplacements of five vibrational modes are 730 cm^{-1}, 0.3; 580 cm^{-1}, 0.3; 435 cm^{-1}, 0.3; 300 cm^{-1}, 0.3; 140 cm^{-1}, 0.5. (a) Solid line: experimental data; long-dashed line: $C(|\omega|<716\ cm^{-1})$, N=0.5; solid structured line in the absorption spectrum: isolated molecule spectrum; a finite linewidth is added for illustration purposes. (b) Diamonds: experimental data; long-dashed line: $C(|\omega|<716\ cm^{-1})$, N=0.5. A pulse ⋯ (as before).

For these two cases, the solvent-solute coupling parameter is reduced to 0.5. The results of Figs. 5 and 8 and the finite breadth of the measured solvent spectral density cannot be used to uniquely determine the range of solvent intramolecular modes that should be included in the simulation to fully describe the solvent-induced fluctuations. Nevertheless, the combination of simulated absorption spectra and echoes compared with the measured signals indicate that both solvent and chromophore intramolecular modes have to be considered.

Following the same calculation procedure, Figs. 9(a) and 9(b) show the experimental and calculated absorption spectra and echo signals of HDITC/DMSO, respectively. The experimental echo was obtained using cavity-dumped laser pulses of 10–15 nJ energies and 100 kHz repetition rate. The reduced repetition rate, hence reduced average power, eliminates any possibility of thermal grating formation in the flowing sample. The best agreement between the experimental and simulated signals is obtained using five displaced harmonic oscillators for the HDITC intra-chromophore vibrations and a solvent-solute coupling parameter of 0.5. The absorption spectrum of HDITC/DMSO is broader than that measured for HITCI/DMSO while the echo signal of the former is narrower than the latter. The differences in spectral widths are due to the different chromophore intramolecular modes but not to the solvent-solute couplings.

E. Time-gated echo simulations

Experimental measurements of the time evolving polarization response as opposed to the time-integrated polarization (i.e., conventional photon echo) response described above have recently been reported by this group[9] and Wiersma's group.[7] The experiments create two controlled periods of evolution in an optical coherence; the system undergoes phase evolution or dephasing in the first period and rephasing in the second. Similar controllable periods of evolution are also obtained by fifth-order three-pulse scattering.[10,11] Here, we calculate the time shift of the polarization response using the spectral density approach described above.

Figure 10(a) shows the time shifts of the time-gated echo peaks as a function of time delay, τ, between the first two pulses. The simulation is for a TLS coupled to the solvent bath for two different ranges of the bath spectral density;

Downloaded¬09¬Sep¬2001¬to¬128.135.233.49.¬Redistribution¬subject¬to¬AIP¬license¬or¬copyright,¬see¬http://ojps.aip.org/jcpo/jcpcr.jsp

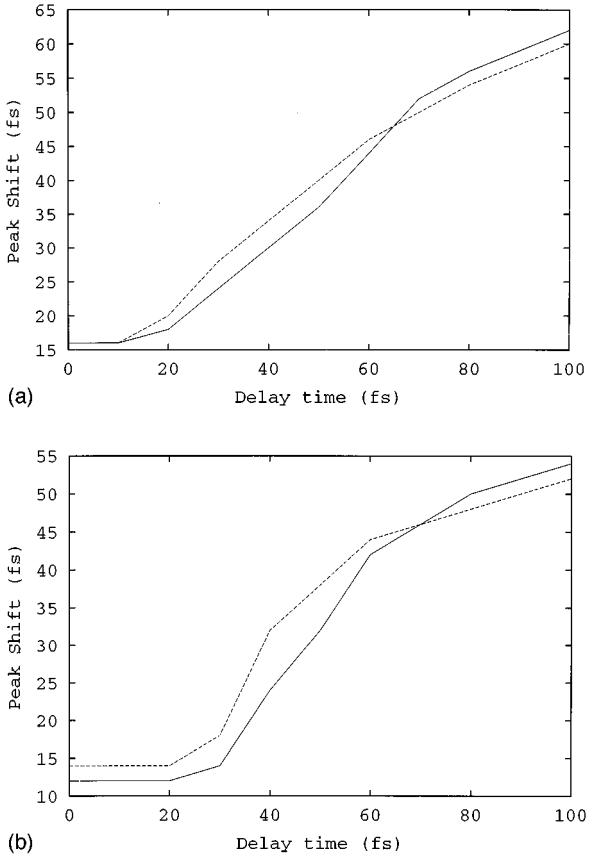

FIG. 10. Calculated peak shift vs time-delay τ in time-gated two-pulse photon echoes. (a) Two-level system. (b) Multi-level system with five chromophore vibrational modes as in Fig. 9. Solid line: $C(|\omega|< 716\ \mathrm{cm}^{-1})$, $N=0.5$. Dashed line: $C(|\omega|< 163\ \mathrm{cm}^{-1})$, $N=0.5$. The pulse duration used is 10 fs.

$|\omega|<163\ \mathrm{cm}^{-1}$ (dashed) and $|\omega|<716\ \mathrm{cm}^{-1}$ (solid). Both curves asymptote to a non-zero value at $\tau=0$ fs and remain flat for 10–12 fs due to convolution effects with finite duration pulses. The solid curve then rises more slowly indicating a more homogeneous bath (i.e., fast frequency modulation). Except for convolution effects, a purely inhomogeneous broadened system would have maximal rephasing when $t=\tau$.

Figure 10(b) is the multimode simulation of the time-gated echo peak shift versus τ associated with the HDITC/DMSO integrated echo of Fig. 9(b). The curves representing the same two spectral density ranges as in Fig. 10(a) now yield different initial time shifts even at $\tau=0$ and are clearly disparate up to a 65–70 fs delay. It is important that the contributions of high and low frequency fluctuations to the polarization response are distinguishable for these shorter delay times since the magnitude of the signal rapidly decreases into the noise level beyond 60 fs or so.[9]

V. DISCUSSION

There are several important points to draw from the comparison of simulation and experimental results presented above. First, the idea of using the OKE spectrum to construct the bath spectral density for optical dephasing has been put on a rigorous theoretical foundation and the approximations involved in its application have been clearly delineated. Second, it was found that the solvent intramolecular modes need to be included in the integrated and time-gated echo calculations to accurately obtain these responses simultaneously with the linear absorption spectrum. Third, the importance of including multiple chromophore vibronic transitions as part of the system was important in simultaneously simulating the same three measured signals. Fourth, the time-gated polarization response (i.e., echo) technique was shown to be a powerful method for distinguishing the form of the intermediate and high frequency solvent responses. These four points will be discussed at greater length in the remainder of this section

A. Echo simulation with a measured spectral density

The clear advantage of the spectral density approach for the simulation of third-order nonlinear responses of chromophores in liquids over the analysis using a single or a finite number of Brownian oscillators (BO)[5,7,11,14] lies in the access to an independent experimental measure of the liquid. A BO analysis does not have any *a priori* constraint into the number or physical nature of the oscillators. The BO approach, however, is flexible and versatile and can give insight into the form of the spectral density.

In the Brownian oscillator model used by Yan and Mukamel[12] a displaced harmonic oscillator is used to describe the effective solvent motions that cause electronic dephasing. Each Brownian oscillator has an associated Stokes-shift, hence a parameter related to the magnitude of the fluctuations (i.e., proportional to coupling strength). In our case, the system-bath coupling is linearly proportional to the solvent nuclear coordinates. As long as the coupling coefficients for the ground state and excited state are different, the electronic energy is modulated. The model for optical dephasing presented in this paper also allows for the situation where the equilibrium position of the solvent nuclear motions might not change; that is, λ can be zero. In this case, fluctuations about a mean exist but no solvation (i.e., displacement from the mean position) would be involved.

A criticism of the OKE spectral density approach described in detail in this paper is that it assumes that the system-bath coupling can be described by a dispersion interaction.[11,52] Symmetric dyes are well known for their large polarizability change on optical excitation without a change in the molecular permanent dipole moment due to equivalent resonance structures.[53] The approach described here could be extended to allow treating dipole-dipole system-bath interactions through the far infrared (i.e., dipolar) spectrum of the pure liquid.[54] We are currently examining chromophores that involve some change in permanent dipole moment on optical excitation to test the generality of this idea.

Another point that should be addressed is the appropriateness of using the depolarized portion of the liquid polarizability spectral density rather than the polarized Raman spectrum. Shuker and Gammon showed[55,56] that the VH Raman spectrum, which is the frequency domain analog of the OKE spectrum, better reflects the calculated density of states

Downloaded¬09¬Sep¬2001¬to¬128.135.233.49. Redistribution subject to AIP license or copyright,¬see¬http://ojps.aip.org/jcpo/jcpcr.jsp

of amorphous glasses. We assume that the depolarized spectrum better reflects the solvent correlation function relevant to optical dephasing (especially the intermolecular solvent spectrum) than the polarized spectrum due to the inherently low symmetry of the system-bath interaction. Clearly, computer simulations of the appropriate spectral density for optical dephasing[57–60] would be useful for comparison with experiments. The ''optimal normal mode'' method recently developed by Voth's group, which facilitates the calculation of time correlation functions in liquids,[27] may be very useful for experimental comparison.

Although a frequency-independent coupling has been used in this paper, three-pulse echo measurements and simulations of the HDITC/DMSO solute-solvent system indicate that the spectral density shown in Fig. 3 is inadequate to simulate slow (i.e., picosecond timescale) spectral diffusion processes.[23] Joo and Fleming[11] have recently shown that slow, that is low frequency, contributions to the system-bath interaction cannot be accounted for by a simple BO analysis but a low frequency component must be added to the spectral density. We have recently shown[61] with a rapid-scan OKE measurement over long times (to 25 ps delay) that even the OKE spectrum itself can significantly underestimate the low frequency region. The amplitude associated with very low frequencies, including liquid self-diffusion, are improperly determined from waveforms of insufficient duration. For mesetylene this difference was an order of magnitude in the range from 2–10 cm^{-1}.[61]

B. Solvent intramolecular modes and optical dephasing

The systematic analysis of solvent contributions to optical dephasing presented above clearly indicates that rapid fluctuations of the bath contribute significantly to the two-pulse photon echo response. The measured spectral density for DMSO contains distinct spectral regions that are associated with solvent inter-molecular and intra-molecular motions. The effect of including these different spectral regions in photon echo simulations clearly indicates that the frequency region of the DMSO intramolecular motions are important for accurate comparison with experiment. These motions can be thought of as fast bath fluctuations. This finding is similar to the conclusion reached by Bardeen and Shank in the echo study of LD690 in n-alcohols.[5] They attributed the fast response of LD690 in n-alcohol to the -OH group librational motion, which is inertial in character because it is the motion of individual molecules, but not to any collective solvent modes.

The magnitude of the solvent intramolecular mode induced fluctuations that a solute senses will depend on the number density of solvent molecules around the solute and the solvent-solute coupling strength. The intensity of the macroscopic measurement of the solvent polarizability response reflects solvent number density. This is why the only parameter left in ''fitting'' the experimental photon echo signal with simulated echo signals, which employ the spectral density obtained by OKE measurement, is the coupling parameter N. By contrast, the intermolecular collective motions are quite slow in the two-pulse photon echo experimental timescale, and their presence mainly causes the echo peak shift.

C. Solute intra-molecular modes

Both the Shank and Wiersma groups have pointed out the importance of including intra-chromophore modes in properly simulating the nonlinear optical signal.[5,15,21] Our approach of using the pump-probe experimental result as opposed to low temperature hole burning spectra[15] or cw-resonance Raman spectra[5,21] to determine vibrational frequencies and displacements is unique. Although the cw-resonance Raman data can yield more precise results for frequencies and displacements, the pump-probe signal gives more self-consistent information about vibrational frequency changes on optical excitation. In the case that chromophores exhibit strong fluorescence, the pump-probe signal will have advantages over the resonance Raman. The analysis method employed here will be discussed in detail elsewhere.[39]

Another interesting aspect of the comparison between simulation and experiment is that consideration of only intra-chromophore modes is not adequate for analysis of the two-pulse echo signals and absorption spectra. Similarly, bath fluctuations are necessary but not sufficient for accurate simulation. The effect of intra-chromophore modes is to cause an initial decrease in the magnitude of the system polarization through evolution of the vibrational superposition state; in the absence of the bath subsequent oscillations would be observed. The solvent bath acts as a dissipation on the vibronic coherence such that these subsequent quantum beats are not observed.

D. N(ω) and time-gated echoes

Frequency independent coupling was assumed in the analysis of time-integrated two-pulse photon echoes presented in this paper. The general validity of this assumption may be further investigated by comparison with the results of time-gated and three-pulse photon echo measurements and simulations.

The time-gated photon echo signals described in Eq. (2) show that the time-gated signal is a convolution integral between the modulus-square of the third-order polarization and the gate pulse intensity. The temporal shape of the third-order polarization can then be directly extracted by deconvolution with the gate pulse. Direct access to $|P^{(3)}(t,\tau)|^2$ more clearly enables the separation of slow and fast modulations (i.e., inhomogeneous and homogeneous broadening) of the electronic energy gap. The time-gating method will therefore be superior to integrated echoes for the elucidation of the optical dephasing spectral density. For instance, the simulation of the time-gated echo signal for different complexity in the system (two-level versus multi-level) and bath (low frequency spectral density versus large frequency range) seen in Figs. 10(a) and 10(b) demonstrates the sensitivity of the echo shape to the form of the bath. Significantly different peak time-shifts of the time-gated polarization response versus pulse separation τ are obtained for different spectral ranges.

Downloaded¬09¬Sep¬2001¬to¬128.135.233.49. Redistribution subject to AIP license or copyright,¬see¬http://ojps.aip.org/jcpo/jcpcr.jsp

Three-pulse (integrated) echo signals, as discussed above, allow access to detection of the slow time-scale spectral diffusion response of the solute-solvent system. This is facilitated by propagating the system in an electronic population (i.e., both bra and ket vectors in the same electronic state) while the solvent continues to fluctuate. The lower frequency motions are then sampled during longer delays (defined as T) between the second and third system-field interactions. The three-pulse experiment is currently being employed to further test the fidelity of the polarizability spectral density to the measured dynamics of optical dephasing and the functional form of the coupling parameter. From experimental and simulation results to be reported elsewhere[23] the spectral density and a frequency independent coupling employed here for two-pulse echoes do not completely describe the intermolecular solvent contributions to optical dephasing. The calculated signals give good fits to the experimental signals with the short delay time T but start to deviate when T is larger than 250 fs. The deviation implies that either the current OKE measurement does not provide an accurate spectral density in low frequency region[61] or the coupling parameter strongly depends on the frequency.

VI. CONCLUSION

We have defined the conditions required for applicability of the polarizability spectral density approach to accurately reflect solute-solvent interactions as observed through the evolution of optical coherence. The bath and solute degrees of freedom that need to be taken into account for accurate simultaneous calculation of multiple experimental measurements were described in detail.

Time-gated three-pulse echo measurements and simulations are currently in progress to map out the frequency dependence of solvent-solute couplings, thereby yielding a form for $N(\omega)$. This effort will more clearly establish the limits of applicability of the physically appealing but perhaps overly simplistic polarizability spectral density model that is rigorously developed in this paper. The extensive amount of information about the bath dynamics causing optical dephasing obtained in these multi-dimensional experiments will provide a strong test for the realistic and accurate first principles simulation of solvent friction in solute-solvent systems. Also, further applicability of the approach using OKE or FIR spectral input will be tested by investigating other solute-solvent systems and through refined experimental techniques.

The ultimate goal of this work is to establish the correct spectral density, or correlation function, that describes solute-bath interactions in liquid media. The transferability of the optical dephasing spectral density to other chromophores (i.e., change λ and $N(\omega)$ but maintain $\mathrm{Im}[\chi_{OKE}(\omega)]$) is being examined.[62,63] Our understanding of solute-bath interactions would benefit from first principles simulations[58–60] that incorporate realistic aspects of the type of chromophore and bath described herein.

ACKNOWLEDGMENTS

We thank Professor Gregory A. Voth for providing us with a preprint of Ref. 27. We thank Dr. Y.-C. Tsai and Dr. L. W. Ungar for enlightening discussions in the theoretical part of this work.

We acknowledge the National Science Foundation for support under grant No. CHE-93-57424, the Deutsche Forschungsgemeinshaft for a postdoctoral fellowship, and the Department of Education for a predoctoral fellowship. NFS is the recipient of David and Lucile Packard Fellowship and an Arnold and Mabel Beckman Foundation Fellowship.

[1] D. A. McQuarrie, in *Statistical Mechanics* (Harper Collins, New York, 1976), Chap. 11.
[2] A. M. Weiner, S. D. Silvestri, and E. P. Ippen, J. Opt. Soc. Am. B **2**, 654 (1985).
[3] Y. S. Bai and M. D. Fayer, Chem. Phys. **128**, 135 (1988).
[4] T. Joo and A. C. Albrecht, Chem. Phys. **176**, 233 (1993).
[5] C. J. Bardeen and C. V. Shank, Chem. Phys. Lett. **226**, 310 (1994).
[6] H. C. Meijers and D. A. Wiersma, J. Chem. Phys. **101**, 6927 (1994).
[7] M. S. Pshenichnikov, K. Duppen, and D. A. Wiersma, Phys. Rev. Lett. **74**, 674 (1995).
[8] M. S. Pshenichnikov, W. P. de Boeij, K. Duppen, and D. A. Wiersma, Chem. Phys. Lett. **238**, 1 (1995).
[9] P. Vöhringer, D. C. Arnett, T.-S. Yang, and N. F. Scherer, Chem. Phys. Lett. **237**, 387 (1995).
[10] M. Cho and G. R. Fleming, J. Phys. Chem. **98**, 3478 (1994).
[11] T. Joo, Y. Jia, and G. R. Fleming, J. Chem. Phys. **102**, 4063 (1995).
[12] Y. Yan and S. Mukamel, J. Chem. Phys. **94**, 179 (1991).
[13] Y. Yan and S. Mukamel, J. Chem. Phys. **89**, 5160 (1988).
[14] W. P. de Boeij, M. S. Pshenichnikov, K. Duppen, and D. A. Wiersma, Chem. Phys. Lett. **224**, 243 (1994).
[15] E. T. J. Nibbering, D. A. Wiersma, and K. Duppen, Chem. Phys. **183**, 167 (1994).
[16] P. Vöhringer, D. C. Arnett, R. A. Westervelt, M. J. Feldstein, and N. F. Scherer, J. Chem. Phys. **102**, 4027 (1995).
[17] D. McMorrow and W. T. Lotshaw, J. Phys. Chem. **95**, 10 395 (1991).
[18] E. W. Castner, Jr., Y. J. Chang, Y. C. Chu, and G. E. Walrafen, J. Chem. Phys. **102**, 653 (1995).
[19] T.-S. Yang, R. Zhang, and A. B. Myers, J. Chem. Phys. **100**, 8573 (1994).
[20] S. R. Hartmann and J. T. Manassah, J. Phys. B **23**, 1363 (1990).
[21] C. J. Bardeen and C. V. Shank, Chem. Phys. Lett. **203**, 535 (1993).
[22] R. W. Schoenlein, D. M. Mittleman, J. J. Shiang, A. P. Alivisatos, and C. V. Shank, Phys. Rev. Lett. **70**, 1014 (1993).
[23] T.-S. Yang, D. C. Arnett, and N. F. Scherer (in preparation).
[24] P. Moore and T. Keyes, J. Chem. Phys. **100**, 6709 (1994).
[25] G. Seeley and T. Keyes, J. Chem. Phys. **91**, 5581 (1989).
[26] R. M. Stratt, Acc. Chem. Res. **28**, 201 (1995).
[27] J. Cao and G. A. Voth, J. Chem. Phys. **103**, 4211 (1995).
[28] A. O. Caldeira and A. J. Leggett, Ann. Phys. **149**, 374 (1983).
[29] A. J. Leggett *et al.*, Rev. Mod. Phys. **59**, 1 (1987).
[30] H. Grabert, P. Schramm, and G.-L. Ingold, Phys. Rev. **168**, 115 (1988).
[31] P. M. Felker and A. H. Zewail, J. Chem. Phys. **86**, 2460 (1987).
[32] J. S. Baskin, P. M. Felker, and A. H. Zewail, J. Chem. Phys. **86**, 2483 (1987).
[33] P. Vöhringer, R. A. Westervelt, T.-S. Yang, D. C. Arnett, M. J. Feldstein, and N. F. Scherer, J. Raman Spectrosc. **26**, 535 (1995).
[34] M. Cho, S. J. Rosenthal, N. F. Scherer, L. D. Ziegler, and G. R. Fleming, J. Chem. Phys. **96**, 5033 (1992).
[35] Y. J. Yan and S. Mukamel, J. Chem. Phys. **86**, 6085 (1987).
[36] M. Cho, M. Du, N. F. Scherer, G. R. Fleming, and S. Mukamel, J. Chem. Phys. **99**, 2410 (1993).
[37] W. T. Pollard, S.-Y. Lee, and R. A. Mathies, J. Chem. Phys. **92**, 4012 (1990).
[38] W. T. Pollard, S. L. Dexheimer, Q. Wang, L. A. Peteanu, C. V. Shank, and R. A. Mathies, J. Phys. Chem. **96**, 6158 (1992).
[39] T.-S. Yang, P. Vöhringer, R. A. Westervelt, and N. F. Scherer (in preparation).

Downloaded¬09¬Sep¬2001¬to¬128.135.233.49. Redistribution subject to AIP license or copyright,¬see¬http://ojps.aip.org/jcpo/jcpcr.jsp

[40] I. A. Walmsley, M. Mitsunaga, and C. L. Tang, Phys. Rev. A **38**, 4681 (1988).
[41] I. A. Walmsley, F. W. Wise, and C. L. Tang, Chem. Phys. Lett. **154**, 315 (1989).
[42] M. T. Asaki, C.-P. Huang, D. Garvey, J. Zhou, H. C. Kapteyn, and M. M. Murnane, Opt. Lett. **18**, 977 (1993).
[43] F. Krausz, Ch. Spielmann, T. Brabec, E. Winter, and A. J. Schmidt, Opt. Lett. **17**, 204 (1992).
[44] D. C. Arnett and N. F. Scherer, Opt. Lett. (in press).
[45] B. Schrader, *Raman/IR Atlas of Organic Compounds* (VCH-Verlag, Weinheim, 1989).
[46] The calculated echo signals are almost the same even if the intensity of $C(\omega=0)$ is increased by an order of magnitude.
[47] W. H. Press, S. A. Teukolsky, W. T. Vetterling, and B. P. Flannery, *Numerical Recipes*, 2nd ed. (Cambridge University, New York, 1992).
[48] E. T. Nibbering, D. A. Wiersma, and K. Duppen, Chem. Phys. **183**, 167 (1994).
[49] H. Sato, M. Kawasaki, K. Kasatani, and M. Katsumata, J. Raman Spectrosc. **19**, 129 (1988).
[50] W. West and A. L. Geddes, J. Phys. Chem. **68**, 837 (1964).
[51] W. T. Pollard, H. L. Fragnito, J.-Y. Bigot, C. V. Shank, and R. A. Mathies, Chem. Phys. Lett. **168**, 239 (1990).
[52] H. P. Deuel, P. Cong, and J. D. Simon, J. Phys. Chem. **98**, 12 600 (1994).
[53] S. R. Marder, C. B. Gorman, F. Meyers, J. W. Perry, G. Bourhill, J.-L. Brédas, and B. M. Pierce, Science **265**, 632 (1994).
[54] P. A. Lund, O. F. Nielsen, and E. Praestgaard, Chem. Phys. **28**, 167 (1978).
[55] R. Shuker and R. W. Gammon, Phys. Rev. Lett. **25**, 222 (1970).
[56] R. Shuker and R. W. Gammon, J. Chem. Phys. **55**, 4784 (1971).
[57] S. J. Rosenthal, B. J. Schwartz, and P. J. Rossky, Chem. Phys. Lett. **229**, 443 (1994).
[58] B. J. Schwartz and P. J. Rossky, J. Phys. Chem. **99**, 2953 (1995).
[59] A. M. Walsh and R. F. Loring, Chem. Phys. Lett. **186**, 77 (1991).
[60] N. E. Shemetulskis and R. F. Loring, J. Chem. Phys. **97**, 1217 (1992).
[61] M. J. Feldstein, P. Vöhringer, and N. F. Scherer, J. Opt. Soc. Am. B **12**, 1500 (1995).
[62] D. Arnett, T.-S. Yang, and N. Scherer, *Time-Resolved Vibrational Spectroscopy-7*, edited by W. Woodruff (in press).
[63] T. S. Yang, D. C. Arnett, L. Book, and N. F. Scherer, J. Phys. Chem. (submitted).

Downloaded¬09¬Sep¬2001¬to¬128.135.233.49. Redistribution subject to AIP license or copyright,¬see¬http://ojps.aip.org/jcpo/jcpcr.jsp